Trigonometric WENO Scheme for Convection-Diffusion Equations

Gulkayer Harman, Kaysar Rahman, and Muyassar Ahmat

***Abstract*—We present a novel fifth-order finite volume trigonometric weighted essentially non-oscillatory (TWENO) scheme for the accurate and robust numerical solution of one-dimensional convection–diffusion equations with potentially non-smooth solutions. The proposed approach reformulates the diffusion term into a first-order system, which is spatially discretized using a nonlinear convex combination of one quartic and two linear trigonometric polynomials within the TWENO framework. Temporal integration is performed using a third-order total variation diminishing (TVD) Runge–Kutta method to ensure stability and accuracy. The primary advantages of the present method are as follows: (1) The scheme allows for the flexible selection of positive linear weights, thereby avoiding the emergence of negative linear weights. (2) Unlike conventional WENO schemes that rely on algebraic polynomials, the use of trigonometric basis functions enhances robustness near discontinuities and improves resolution properties. Extensive numerical experiments are conducted to verify the effectiveness of the proposed method, demonstrating its superior accuracy, non-oscillatory behavior, and high-resolution capability in capturing sharp gradients and discontinuities.**

***Index Terms*—TWENO scheme, Finite volume scheme, Convection-diffusion equation, TVD Runge-Kutta method.**

I. Introduction

THE Convection-diffusion equation is a crucial partial differential equation. It models various physical processes, such as heat transfer in thin films, dispersion of dissolved substances, and solute transport in liquids. As a result, it is of great significance in numerous fields, especially in environmental science and fluid mechanics. In recent decades, several methods have been utilized to solve the convection-diffusion equations, including finite difference methods [1], finite element methods [2], and finite volume methods [3]. When diffusion is the dominant factor, these equations show elliptic or parabolic behavior. In such cases, classical finite difference and finite element methods can provide stable and accurate solutions. However, in convection-dominated scenarios where the equations exhibit hyperbolic characteristics, conventional numerical methods often encounter spurious oscillations and instability when dealing with discontinuities or sharp gradients. To address these challenges, advanced numerical methods have been introduced in [4], [5], etc. Furthermore, the weighted essentially non-oscillatory (WENO) scheme is widely recognized as an effective technique for shock capturing, particularly in the numerical solutions of hyperbolic conservation laws and related Hamilton-Jacobi equations. Over the past years, researchers have extensively applied this method to handle the hyperbolic conservation laws and first-derivative convection terms in convection-dominated convection-diffusion partial differential equations. Therefore, the WENO method is suitable for solving convection-diffusion equations. In 1994, Liu et al. [6] developed an improved WENO scheme within the finite volume framework. This scheme enhanced the kth-order accuracy of the ENO scheme to the $(k+1)$th-order accuracy in smooth regions. Subsequently, Jiang and Shu [7] proposed an arbitrary $(2k-1)$th-order accurate finite difference WENO scheme and presented a framework for designing smoothness indicators and nonlinear weights, which is applicable to both finite difference and finite volume WENO methods. Since then, numerous efficient WENO schemes for hyperbolic conservation law equations have been proposed using the idea of reconstruction [8], [9], [10], etc.

The development of trigonometric polynomial based reconstruction has significantly advanced the field of numerical methods. Early work by Baron[11] introduced Neville's trigonometric interpolation. However, this approach was not directly applicable for constructing higher-order ENO schemes. In 1996, Christofi[12] proposed a method for local trigonometric polynomial interpolation, which enabled the progressive addition of interpolation points, paving the way for the formulation of advanced trigonometric ENO methods. More recently, Zhu and Qiu[13] developed a fifth-order trigonometric WENO method specifically designed to handle highly oscillatory problems. Building on this foundation, a new scheme[14] was introduced as a limiter for the Runge–Kutta discontinuous Galerkin (RKDG) method, utilizing the same class of trigonometric polynomials as in [13]. Overall, these trigonometric polynomial–based schemes have demonstrated excellent performance both in smooth solution regions and in the vicinity of contact discontinuities.

Subsequently, based on the reconstruction idea, Liu et al. [15] proposed the direct finite difference WENO (DWENO) scheme for solving nonlinear degenerate parabolic equations. In this method, the diffusion flux is directly approximated by a conservative flux difference. However, the scheme still faces some challenges, such as the use of nonlinear mapped weights and negative linear weights. To avoid the emergence of negative ideal weights and mapped nonlinear weights, Jiang [16] proposed a finite difference multi-resolution (MR-WENO) scheme for solving degenerate parabolic equations. This method allows the linear weights to be set as any positive numbers whose sum is 1, thereby enhancing the flexibility and stability of the numerical scheme. After that,

Manuscript received January 12, 2025; revised June 12, 2025.
This work was supported by the Natural Science Foundation of Xinjiang Uygur Autonomous Region of China under Grant 2024D01C43 and Talent Project of Tianchi Doctoral Program in Xinjiang Uygur Autonomous Region of China under Grant 5105240152t.

Gulkayer Harman is a Master's Student of College of Mathematics and Systems Science, Xinjiang University, Urumqi, Xinjiang, 830017, China (e-mail: gulikayer@163.com).

Kaysar Rahman is an Associate Professor of College of Mathematics and Systems Science, Xinjiang University, Urumqi, Xinjiang, 830017, China (Corresponding author; e-mail: kaysar106@xju.edu.cn).

Muyassar Ahmat is an Associate Professor of College of Mathematics and Systems Science, Xinjiang University, Urumqi, Xinjiang, 830017, China (email: Muyassar@xju.edu.cn).

Ahmat et al. [17] introduced a sixth-order finite difference HWENO scheme, which requires only four points in the reconstruction procedure, resulting in remarkable compactness and accuracy.

Inspired by the concept that any set of positive linear weights (summing to 1) can be used in WENO schemes [10], and considering that trigonometric WENO schemes [13], [14] are more robust and have more advantages in handling complex problems, we propose a finite volume trigonometric WENO scheme to solve the convection-diffusion equation.

This paper is organized as follows: Section II describes the construction of the trigonometric WENO scheme in detail. Section III displays the numerical test results of the present method. Section IV provides the conclusion.

II. Description of Finite Volume trigonometric WENO scheme

In this study, we address the numerical solution of the convection–diffusion equation, formulated as follows:

$$v_t + s(v)_x = z(v)_{xx}, \quad (x,t) \in [x_l, x_r] \times [0,t], \tag{1}$$

with the initial condition:

$$v(x,0) = v_0(x), \tag{2}$$

where $v := v(x,t)$. Then, we transform equation (1) as a nonlinear system of first-order equations:

$$\begin{cases} v_t + s(v)_x = w_x, \\ w = z(v)_x. \end{cases} \tag{3}$$

For simplicity, we take a uniform mesh on the interval $[x_l, x_r]$, where the target cell is $S_k = [x_{k-\frac{1}{2}}, x_{k+\frac{1}{2}}]$ with a width h. By integrating (3) over the cell S_k, we obtain

$$\begin{cases} \dfrac{d\bar{v}(x_k,t)}{dt} = -\dfrac{1}{h}\big(s(v(x_{k+\frac{1}{2}},t)) - s(v(x_{k-\frac{1}{2}},t))\big), \\ \qquad\qquad + \dfrac{1}{h}\big(w(v(x_{k+\frac{1}{2}},t)) - w(v(x_{k-\frac{1}{2}},t))\big), \\ \bar{w}(x_k,t) = \dfrac{1}{h}\big(z(v(x_{k+\frac{1}{2}},t)) - z(v(x_{k-\frac{1}{2}},t))\big), \end{cases} \tag{4}$$

where

$$\begin{cases} \bar{v}_k(t) = \dfrac{1}{h}\displaystyle\int_{I_k} v(\eta,t)\mathrm{d}\eta, \\ \bar{w}_k(t) = \dfrac{1}{h}\displaystyle\int_{I_k} w(\eta,t)\mathrm{d}\eta. \end{cases}$$

are the cell averages. We approximate (4) using the following conservative scheme:

$$\begin{cases} \dfrac{d\bar{v}_k(t)}{dt} = -\dfrac{1}{h}\big(\hat{s}_{k+\frac{1}{2}} - \hat{s}_{k-\frac{1}{2}}\big) + \dfrac{1}{h}\big(\hat{w}_{k+\frac{1}{2}} - \hat{w}_{k-\frac{1}{2}}\big), \\ \bar{w}_k = \dfrac{1}{h}\big(\hat{z}_{k+\frac{1}{2}} - \hat{z}_{k-\frac{1}{2}}\big). \end{cases}$$

where $\bar{v}_k(t)$ and $\bar{w}_k(t)$ are the numerical approximations to the cell averages $\bar{v}\,(x_k,t)$ and $\bar{w}\,(x_k,t)$, respectively. The numerical flux $\hat{s}_{k+\frac{1}{2}}$ is defined with Lax-Friedrichs flux as:

$$\hat{s}_{k+\frac{1}{2}} = \frac{1}{2}\big(s(v^+_{k+\frac{1}{2}}) + s(v^-_{k+\frac{1}{2}}) - \alpha(v^+_{k+\frac{1}{2}} - v^-_{k+\frac{1}{2}})\big),$$

where $\alpha = \max_v |s'(v)|$. For the numerical fluxes $\hat{w}_{k+\frac{1}{2}}$ and $\hat{z}_{k+\frac{1}{2}}$, we adopt an alternating flux [18] as follows:

$$\hat{w}_{k+\frac{1}{2}} = w^-_{k+\frac{1}{2}}, \quad \hat{z}_{k+\frac{1}{2}} = z^+_{k+\frac{1}{2}}.$$

The values $v^{\pm}_{k+\frac{1}{2}}$ will be achieved by the fifth-order finite volume trigonometric WENO reconstruction. Now we describe fifth-order accurate reconstruction procedures for $v^-_{k+\frac{1}{2}}$.

Step 1. We select three stencils of different sizes to reconstruct trigonometric polynomials with varying degrees. Using the symmetric stencil $\mathcal{S}_1 = \{S_{k-2}, S_{k-1}, S_k, S_{k+1}, S_{k+2}\}$, we reconstruct a quartic trigonometric polynomial $p_1(x) \in \mathrm{span}\{1, \sin(x - x_k), \cos(x - x_k) - \frac{\sin(\frac{h}{2})}{\frac{h}{2}}, \sin(2(x - x_k)), \cos(2(x - x_k)) - \frac{\sin(h)}{h}\}$:

$$\begin{aligned} p_1(x) = a_0 &+ a_1 \sin(x - x_k) + a_2(\cos(x - x_k) - \frac{\sin(\frac{h}{2})}{\frac{h}{2}}) \\ &+ a_3 \sin(2(x - x_k)) + a_4(\cos(2\,(x - x_k)) - \frac{\sin(h)}{h}), \end{aligned}$$

which satisfy

$$\frac{1}{h}\int_{S_{k+l}} p_1(x)dx = \bar{v}_{k+l}, \quad l = -2,-1,0,1,2, \tag{5}$$

where $\bar{v}_{k+l} := \bar{v}(x_{k+l})$ and the coefficients $a_0, \ldots, a_4$ are undetermined. For simplicity, we set $x_k = 0$. Then, by solving the linear system (5), we can derive the coefficients as follows:

$$\begin{aligned} a_0 &= \bar{v}_k, \\ a_1 &= \frac{h\csc^4\left(\frac{h}{2}\right)\sec\left(\frac{h}{2}\right)}{64\cos(h) + 32}\big(2\cos(2h)\bar{v}_{k-1} - 2\cos(2h)\bar{v}_{k+1} \\ &\quad - \bar{v}_{k-2} + \bar{v}_{k+2}\big), \\ a_2 &= -\frac{h\csc^5\left(\frac{h}{2}\right)}{64\cos(h) + 32}\big(-4\cos^2(h)\bar{v}_{k-1} + 4\cos(2h)\bar{v}_k \\ &\quad - 2\cos(2h)\bar{v}_{k+1} + \bar{v}_{k-2} + 2\bar{v}_k - 2\bar{v}_{k+1} + \bar{v}_{k+2}\big), \\ a_3 &= \frac{h\csc^4\left(\frac{h}{2}\right)\sec^2\left(\frac{h}{2}\right)}{64(2\cos(h) + 1)}\big(\sec(h)\bar{v}_{k-2} - \sec(h)\bar{v}_{k+2} \\ &\quad - 2\bar{v}_{k-1} + 2\bar{v}_{k+1}\big), \\ a_4 &= \frac{h\csc^5\left(\frac{h}{2}\right)\sec^3\left(\frac{h}{2}\right)}{128(2\cos(h) + 1)}\big(-2(\cos(h) + 1)\bar{v}_{k-1} \\ &\quad + 4\cos(h)\bar{v}_k - 2\cos(h)\bar{v}_{k+1} + \bar{v}_{k-2} \\ &\quad + 2\bar{v}_k - 2\bar{v}_{k+1} + \bar{v}_{k+2}\big). \end{aligned}$$

On the other two stencils $\mathcal{S}_2 = \{S_{k-1}, S_k\}$ and $\mathcal{S}_3 = \{S_k, S_{k+1}\}$, we reconstruct two linear trigonometric polynomials $p_2(x), p_3(x) \in \mathrm{span}\,\{1, \sin\,(x - x_k)\}$:

$$\begin{aligned} p_2(x) &= b_0 + b_1 \sin(x - x_k), \\ p_3(x) &= c_0 + c_1 \sin(x - x_k), \end{aligned}$$

which satisfy

$$\begin{aligned} \frac{1}{h}\int_{S_{k+l}} p_2(x)dx &= \bar{v}_{k+l}, \quad l = -1, 0, \\ \frac{1}{h}\int_{S_{k+l}} p_3(x)dx &= \bar{v}_{k+l}, \quad l = 0, 1. \end{aligned}$$

where b_0, b_1 and c_0, c_1 are the coefficients of p_2 and p_3, respectively. Similarly, the coefficients can be calculated as:

$$\begin{aligned} b_0 &= \bar{v}_k, \\ b_1 &= -\frac{1}{2}h\csc\left(\frac{h}{2}\right)\csc(h)\left(\bar{v}_{k-1} - \bar{v}_k\right), \end{aligned}$$

$$c_0 = \bar{v}_k,$$
$$c_1 = -\frac{1}{2}h\csc\left(\frac{h}{2}\right)\csc(h)\left(\bar{v}_k - \bar{v}_{k+1}\right).$$

Substituting the coefficients into the polynomial expressions, we can compute $p_1(x)$, $p_2(x)$, and $p_3(x)$. Then, the values of these polynomials at $x_{k+\frac{1}{2}}$ are obtained as follows:

$$\begin{aligned} p_1(x_{k+\frac{1}{2}}) &= \frac{1}{h}\big(a_0 h + a_1 h\sin\left(\frac{h}{2}\right) - 2a_2\sin\left(\frac{h}{2}\right) \\ &\quad + a_3 h\sin(h)\big), \\ p_2(x_{k+\frac{1}{2}}) &= b_0 + b_1\sin\left(\frac{h}{2}\right), \\ p_3(x_{k+\frac{1}{2}}) &= c_0 + c_1\sin\left(\frac{h}{2}\right). \end{aligned}$$

Step 2. Now, we rewrite $p_1(x_{k+\frac{1}{2}})$ as:

$$\begin{aligned} p_1(x_{k+\frac{1}{2}}) = \gamma_1\Big(\frac{1}{\gamma_1}p_1(x_{k+\frac{1}{2}}) - \frac{\gamma_2}{\gamma_1}p_2(x_{k+\frac{1}{2}}) - \frac{\gamma_3}{\gamma_1}p_3(x_{k+\frac{1}{2}})\Big) \\ + \gamma_2 p_2(x_{k+\frac{1}{2}}) + \gamma_3 p_3(x_{k+\frac{1}{2}}). \end{aligned} \tag{6}$$

where $\gamma_1, \gamma_2, \gamma_3$ are linear weights. Note that, in equation (6) , as long as the denominator $\gamma_1 \neq 0$, it holds for any positive weight set $\gamma_1, \gamma_2, \gamma_3$ satisfying the condition $\sum_{i=1}^{3}\gamma_i = 1$. In this study, we set $\gamma_1 = 0.98$, $\gamma_2 = \gamma_3 = 0.01$.

Step 3. Calculate the smoothness indicators $\beta_{ll}(ll = 1, 2, 3)$. These indicators are used to measure the smoothness of the polynomial $p_{ll}(x)$ within the computational cell I_k. The smaller these smoothness indicators, the smoother the function is within I_k. Using the classic method of calculating smoothness indicators given in the literature [7]:

$$\beta_{ll} = \sum_{m=1}^{r}\int_{S_k} h^{2m-1}\Big(\frac{d^m p_{ll}(x)}{dx^m}\Big)^2 dx, \quad ll = 1, 2, 3, \tag{7}$$

where $r = 4$ for $ll = 1$, while $r = 1$ for $ll = 2$ or $ll = 3$. By substituting the expression of p_{ll} into (7), we obtain:

$$\begin{aligned} \beta_1(x) = &-\frac{8}{3}a_3 a_1 h(4h^4+1)\sin\left(\frac{h}{2}\right)\big((2h^2-1)\cos(h) \\ &-2(h^2+1)\big) + \frac{8}{3}a_2 a_4 h(4h^4+1)\sin\left(\frac{h}{2}\right)\big(4h^2 \\ &+(2h^2-1)\cos(h)+1\big) + \frac{1}{2}a_1^2 h(h^4+1)\big(h^3 \\ &-h^2\sin(h)+h+\sin(h)\big) + \frac{1}{2}a_2^2 h(h^4+1)\big(h^3 \\ &+(h^2-1)\sin(h)+h\big) + 2a_3^2 h(16h^4+1)\big(4h^3 \\ &+(1-4h^2)\sin(h)\cos(h)+h\big) + 2a_4^2 h(16h^4 \\ &+1)\big(4h^3+(4h^2-1)\sin(h)\cos(h)+h\big), \\ \beta_2(x) = &\frac{1}{2}b_1^2 h(h+\sin(h)), \\ \beta_3(x) = &\frac{1}{2}c_1^2 h(h+\sin(h)). \end{aligned}$$

Step 4. To introduce the nonlinear weights $\omega_{ll}(ll = 1, 2, 3)$, first measure the absolute difference of smoothness indicators as follows:

$$\tau = \frac{1}{4}(|\beta_1 - \beta_2| + |\beta_1 - \beta_3|)^2,$$

Then the specific definition of the nonlinear weights ω_{ll} is shown as follows:

$$\omega_{ll} = \frac{\breve{\omega}_{ll}}{\sum_{m=1}^{3}\breve{\omega}_m}, \quad \breve{\omega}_{ll} = r_{ll}\left(1 + \frac{\tau}{\varepsilon + \beta_{ll}}\right), \quad ll = 1, 2, 3.$$

Here, ϵ is a relatively small positive number introduced to avoid the denominator becoming zero. We set $\epsilon = 10^{-10}$ in all our numerical tests.

Step 5. We replace the linear weights in equation (6) with the nonlinear weights from equation (II), so that we can obtain

$$\begin{aligned} v^{-}_{k+\frac{1}{2}} = &\omega_1\Big(\frac{1}{\gamma_1}p_1(x_{k+\frac{1}{2}}) - \frac{\gamma_2}{\gamma_1}p_2(x_{k+\frac{1}{2}}) - \frac{\gamma_3}{\gamma_1}p_3(x_{k+\frac{1}{2}})\Big) \\ &+ \omega_2 p_2(x_{k+\frac{1}{2}}) + \omega_3 p_3(x_{k+\frac{1}{2}}). \end{aligned} \tag{8}$$

Similarly, we use the mirror symmetry to obtain the reconstruction of $v^{+}_{k+\frac{1}{2}}$.

Finally, after spatial discretization, we solve the semi-discretization (II) using the third-order TVD Runge–Kutta method [19] and obtain :

$$\begin{cases} v^{(1)} = v^n + \Delta t\mathcal{L}(v^n), \\ v^{(2)} = \frac{3}{4}v^n + \frac{1}{4}v^{(1)} + \frac{1}{4}\Delta t\mathcal{L}(v^{(1)}), \\ v^{n+1} = \frac{1}{3}v^n + \frac{2}{3}v^{(2)} + \frac{2}{3}\Delta t\mathcal{L}(v^{(2)}). \end{cases} \tag{9}$$

III. Numerical tests

In this section, we provide numerical tests to exhibit that the proposed method has high-order accuracy and performs well in capturing sharp fronts. For stability, we define the time step as:

$$\Delta t = \frac{CFL}{\frac{\max|s'(v)|}{h} + \frac{\max|z'(v)|}{h^2}}$$

with $CFL = 0.4$.

Additionally, we consider three numerical methods for comparison: the present TWENO scheme, DWENO scheme [15], MRWENO scheme [16]. Finally, we define the error and convergence order as follows:

$$\begin{aligned} L^1\text{error} &= \frac{1}{N}\sum_{k=1}^{N}|v_k^n - V_k|, \\ L^\infty\text{error} &= \max_{1\le k\le N}|v_k^n - V_k|, \\ L^2\text{error} &= \sqrt{\frac{1}{N}\sum_{k=1}^{N}|v_k^n - V_k|^2}, \\ \text{Order} &= \log_2\left(\frac{E_N}{E_{2N}}\right). \end{aligned}$$

Here, v_k is the numerical solution, and V_k is the exact solution. E_N and E_{2N} are the L^1, L^∞, or L^2 errors when using N and $2N$ elements, respectively.

A. Example 1

We test the accuracy of the fifth-order finite volume scheme on the linear equation:

$$v_t + v_x = v_{xx}, \quad 0 \le x \le 2\pi,$$

with the initial condition:

$$v(x,0) = sin(x),$$

and periodic boundary condition. The analytical solution is

$$v(x,t) = e^{-t}\sin(x-t).$$

Table I presents the numerical errors and convergence orders achieved using the TWENO scheme at time $t = 2$. As can be observed, TWENO method can achieve fifth-order accuracy in the smooth region.

TABLE I
THE L^∞, L^1 AND L^2 NORM ERRORS AND CONVERGENCE ORDERS.

N	L^∞ error	order	L^1 error	order	L^2 error	order
10	5.52 e-05		3.57 e-05		4.08 e-05	
20	1.66 e-06	5.04	1.07 e-06	5.05	1.18 e-06	5.10
40	3.81 e-08	5.44	2.43 e-08	5.46	2.70 e-08	5.46
80	7.34 e-10	5.69	4.67 e-10	5.69	5.19 e-10	5.69

B. Example 2

In the following, we consider the Burgers equation:

$$v_t + (\frac{v^2}{2})_x = \frac{1}{Re}v_{xx}, \quad 0 \le x \le 1,$$

with the initial condition:

$$v(x,0) = sin(\pi x).$$

The boundary conditions $v(0,t) = 0$ and $v(1,t) = 0$ are considered in this example. Here, Re denotes the Reynolds number. We show that the numerical solutions for $Re = 1, 10, 100, 10000$ exhibit the correct physical behavior at different times in Figure 1. Notice that as the Reynolds number increases, the propagation front becomes steeper. Figure 2 presents numerical solutions at $Re = 10000, Re = 20000$ and $t = 0.6$. We observe that there are non-physical oscillations present in the numerical solutions in regions with large gradients.

C. Example 3

We study the Buckley-Leverett equation of the form (1). The diffusion flux $z(v)$ is defined as follows:

$$z(v) = \begin{cases} 0, & v < 0, \\ \epsilon\left(2v^2 - \frac{4}{3}v^3\right), & 0 \le v \le 1, \\ \frac{2}{3}\epsilon, & v > 1. \end{cases} \tag{10}$$

We consider the advection flux $s(v)$ to have an s-shaped form given by

$$s(v) = \frac{v^2}{v^2 + (1-v)^2}, \tag{11}$$

as well as the flux $s(v)$ with gravitational effects

$$s(v) = \frac{v^2}{v^2 + (1-v)^2}\left(1 - 5(1-v)^2\right). \tag{12}$$

Initially, we simulate the initial-boundary value problem using the fluxes defined in equations (10), (11). The initial data is considered as

$$v(x,0) = \begin{cases} 1 - 3x, & 0 \le x \le \frac{1}{3}, \\ 0, & \frac{1}{3} < x \le 1, \end{cases}$$

with the boundary condition $v(0,t) = 1$. In Figure 3 we present the results for three WENO schemes with $N = 200$ at different times. Here, the reference solutions are computed by using the HWENO scheme [17] for all computations. We can notice that the TWENO scheme demonstrates better results and higher efficiency in this test case.

Subsequently, we simulate the Buckley-Leverett equation using the fluxes (10),(11) and (10),(12). The initial condition for this Riemann problem is given by:

$$v(x,0) = \begin{cases} 0, & 0 \le x < 1 - \frac{1}{\sqrt{2}}, \\ 1, & 1 - \frac{1}{\sqrt{2}} \le x \le 1, \end{cases}$$

with boundary conditions $v(0,t) = 0$ and $v(1,t) = 1$. Figures 4 and 5 display the numerical solutions for the three schemes at different times with $N = 200$. In this example, the TWENO scheme yields good results and higher resolution in this example.

D. Example 4

In this final test, we solve the strongly degenerate parabolic equation of the form (1), we take the diffusion flux as $s(v) = \epsilon v^2$ with $\epsilon = 0.01$ and the advection flux as

$$z(v) = \begin{cases} \varepsilon(v + 0.25), & v < -0.25 \\ \varepsilon(v - 0.25), & v > 0.25 \\ 0, & |v| \le 0.25 \end{cases}$$

with initial conditions

$$v(x,0) = \begin{cases} 1, & -\frac{1}{\sqrt{2}} - 0.4 < x < -\frac{1}{\sqrt{2}} + 0.4, \\ -1, & \frac{1}{\sqrt{2}} - 0.4 < x < \frac{1}{\sqrt{2}} + 0.4, \\ 0, & \text{otherwise .} \end{cases}$$

The boundary condition is $v(\pm 2, t) = 0$ considered in this case. The numerical results for the three methods at different time levels with $N = 400$ grid points are shown in Figure 6. The TWENO scheme exhibits optimal performance across varying time intervals in this test case.

IV. CONCLUSION

The proposed fifth-order finite volume TWENO scheme demonstrates superior accuracy, robustness, and resolution when solving one-dimensional convection-diffusion equations with non-smooth solutions. By leveraging trigonometric polynomial reconstructions and an effective temporal discretization via the third-order TVD Runge-Kutta method. The method not only overcomes challenges associated with negative weights but also enhances stability near discontinuities. Numerical experiments confirm the scheme's high-order convergence and its potential as a powerful tool for complex problems. Moreover, it is adaptable for the numerical computation of multi-dimensional convection-diffusion equations.

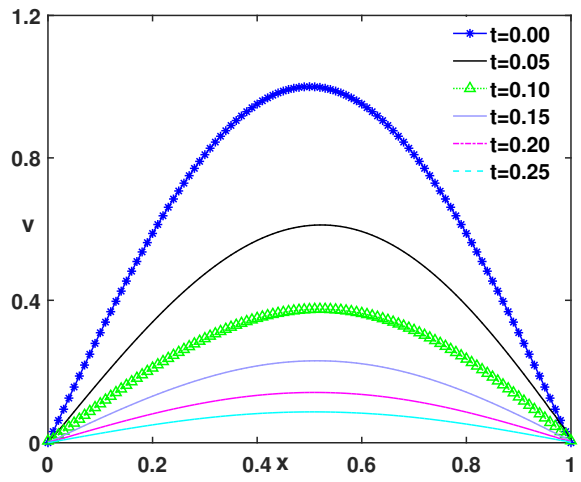

(a) $Re = 1$

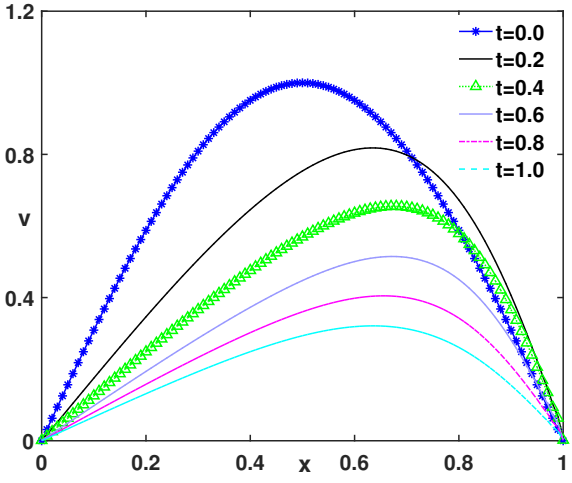

(b) $Re = 10$

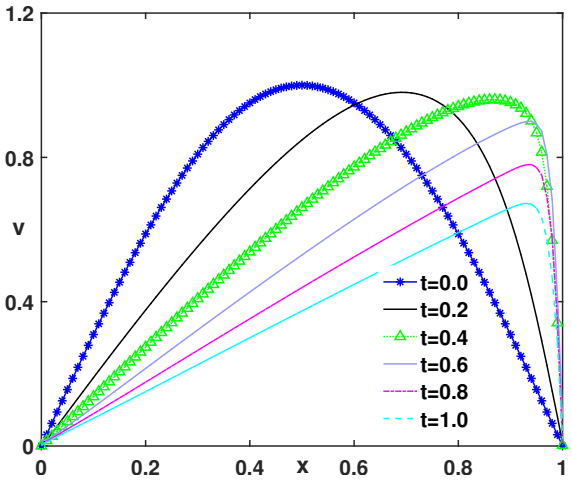

(c) $Re = 100$

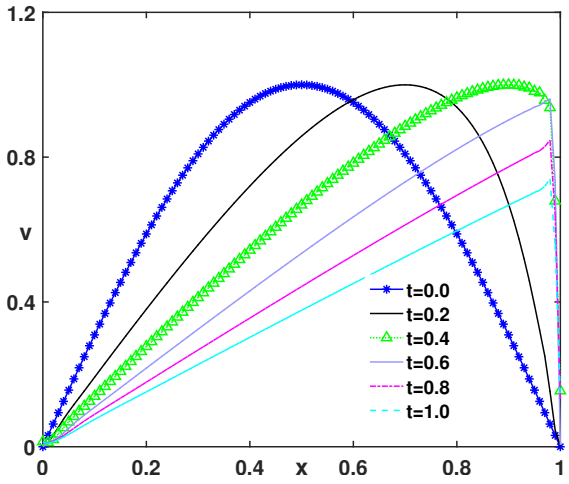

(d) $Re = 10000$

Fig. 1. Example 2. Numerical solutions for the Burgers equation at different times and Reynolds numbers. (a) $Re = 1$,(b) $Re = 10$,(c) $Re = 100$,(d) $Re = 10000$.

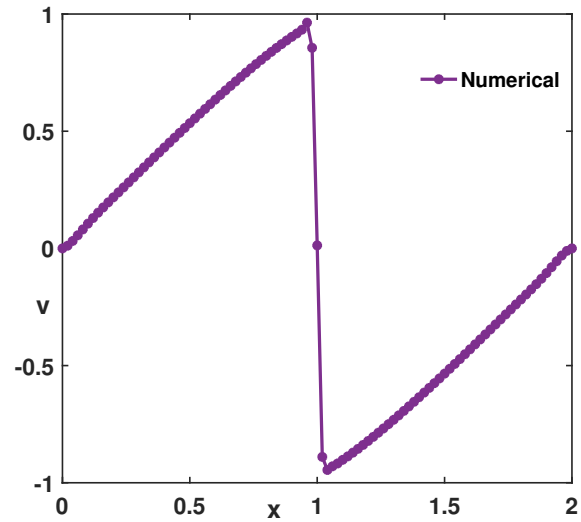

(a) $Re = 10000, t = 0.6$

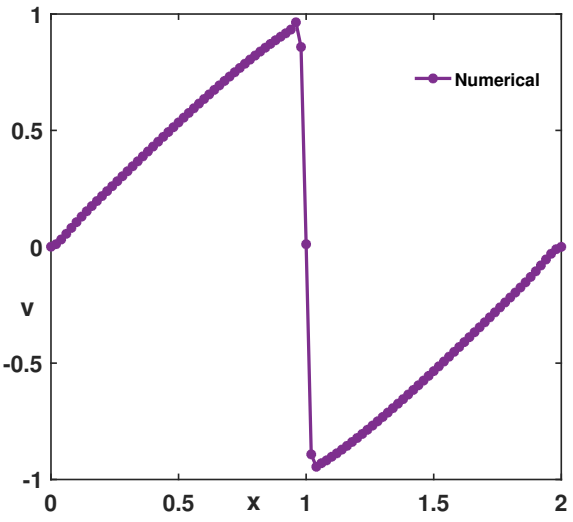

(b) $Re = 20000, t = 0.6$

Fig. 2. Example 2. Numerical solutions for the Burgers equation at $t = 0.6$ and $Re = 10000, 20000$.(a) $Re = 10000, t = 0.6$,(b) $Re = 20000, t = 0.6$.

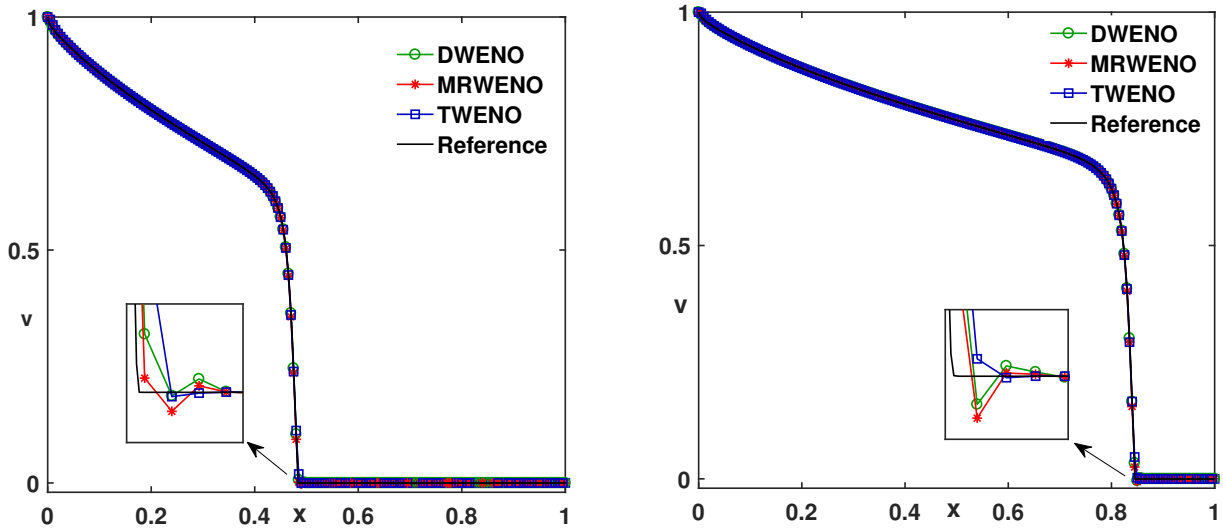

(a) $t = 0.2$ (b) $t = 0.5$

Fig. 3. Example 3. The solution of the Buckley–Leverett equation at $t = 0.2$ and $t = 0.5$, using $N = 200$.(a) $t = 0.2$,(b) $t = 0.5$.

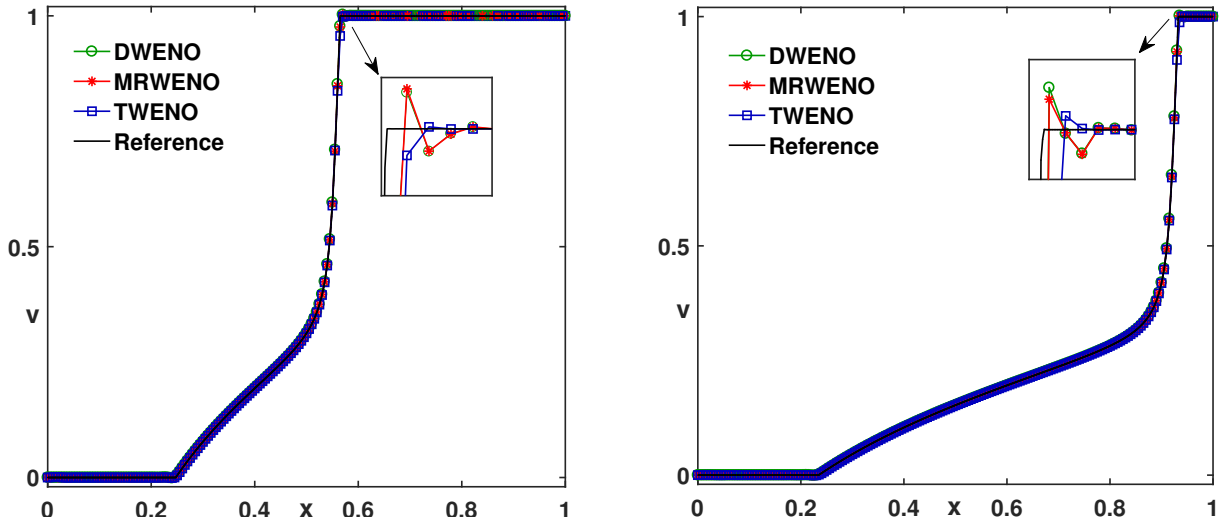

(a) $t = 0.2$ (b) $t = 0.5$

Fig. 4. Example 3. The solution of the Buckley–Leverett equation at $t = 0.2$ and $t = 0.5$, using $N = 200$.(a) $t = 0.2$,(b) $t = 0.5$.

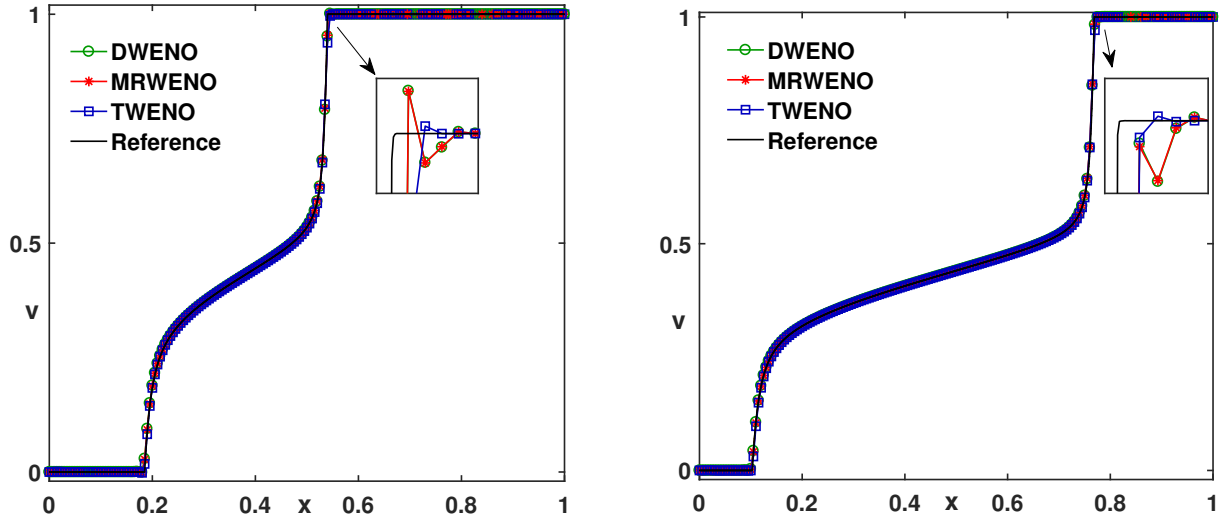

(a) $t = 0.1$ (b) $t = 0.2$

Fig. 5. Example 3. The solution of the Buckley–Leverett equation at $t = 0.1$ and $t = 0.2$, using $N = 200$.(a) $t = 0.1$,(b) $t = 0.2$.

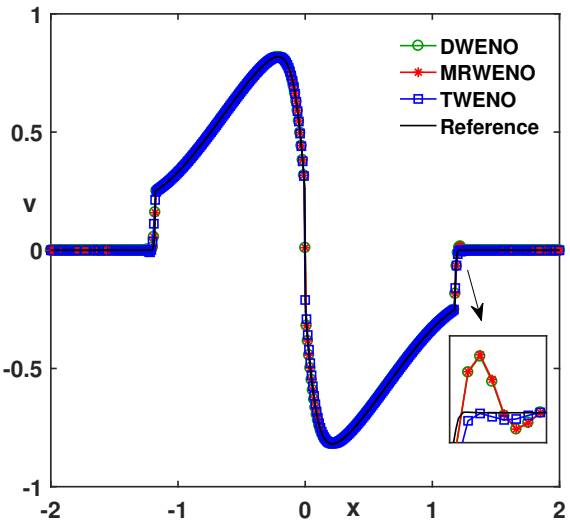

(a) $t = 0.4$

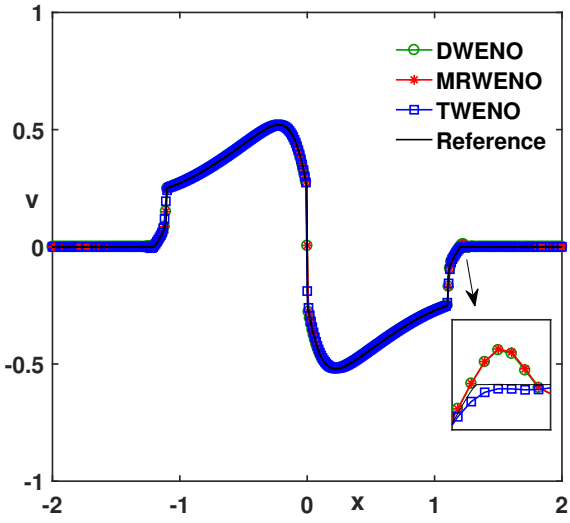

(b) $t = 0.8$

Fig. 6. Example 4. The solution of the strongly degenerate parabolic equation at $t = 0.4, 0.8$, using $N = 400$.(a) $t = 0.4$,(b) $t = 0.8$.

REFERENCES

[1] M. Dehghan and A. Mohebbi, "High-order compact boundary value method for the solution of unsteady convection–diffusion problems," *Mathematics and Computers in Simulation*, vol. 79, no. 3, pp. 683–699, 2008.

[2] R. Lin, X. Ye, S. Zhang, and P. Zhu, "A weak galerkin finite element method for singularly perturbed convection-diffusion–reaction problems," *SIAM Journal on Numerical Analysis*, vol. 56, no. 3, pp. 1482–1497, 2018.

[3] C. Cancès, C. Chainais-Hillairet, A. Gerstenmayer, and A. Jüngel, "Finite-volume scheme for a degenerate cross-diffusion model motivated from ion transport," *Numerical Methods for Partial Differential Equations*, vol. 35, no. 2, pp. 545–575, 2019.

[4] Y. Cheng and C. W. Shu, "Superconvergence of discontinuous galerkin and local discontinuous galerkin schemes for linear hyperbolic and convection-diffusion equations in one space dimension," *Siam Journal on Numerical Analysis*, vol. 47, no. 6, pp. 4044–4072, 2010.

[5] Shu and Chi-Wang, "High order weighted essentially nonoscillatory schemes for convection dominated problems," *Siam Review*, vol. 51, no. 1, pp. 82–126, 2009.

[6] X. D. Liu, S. Osher, and T. Chan, "Weighted essentially non-oscillatory schemes," *Journal of Computational Physics*, vol. 115, no. 1, pp. 200–212, 1994.

[7] G.-S. Jiang and C.-W. Shu, "Efficient implementation of weighted eno schemes," *Journal of computational physics*, vol. 126, no. 1, pp. 202–228, 1996.

[8] D. Levy, G. Puppo, and G. Russo, "Compact central weno schemes for multidimensional conservation laws," *SIAM Journal on Scientific Computing*, vol. 22, no. 2, pp. 656–672, 2000.

[9] J. Qiu and C. W. Shu, "Hermite weno schemes and their application as limiters for runge-kutta discontinuous galerkin method: one-dimensional case," *Journal of Computational Physics*, vol. 193, no. 1, pp. 115–135, 2004.

[10] J. Zhu and J. Qiu, "A new type of finite volume weno schemes for hyperbolic conservation laws," *Journal of Scientific Computing*, no. 5, pp. 1–22, 2017.

[11] J. P. Berrut, "Baryzentrische formeln zur trigonometrischen interpolation (i)," *Ztschrift für angewandte Mathematik und Physik ZAMP*, vol. 35, no. 1, pp. 91–105, 1984.

[12] S. N. Christofi, *The study of building blocks for essentially non-oscillatory (ENO) schemes*. Brown University, 1996.

[13] J. Zhu and J. Qiu, "Trigonometric weno schemes for hyperbolic conservation laws and highly oscillatory problems," *Communications in Computational Physics*, vol. 8, no. 5, pp. 1242–1263, 2010.

[14] G. Sci, "A new fifth-order trigonometric weno scheme for hyperbolic conservation laws and highly oscillatory problems," *Advances in Applied Mathematics and Mechanics*, vol. 11, no. 5, pp. 1114–1135, 2019.

[15] Y. Liu, C.-W. Shu, and M. Zhang, "High order finite difference weno schemes for nonlinear degenerate parabolic equations," *SIAM Journal on Scientific Computing*, vol. 33, no. 2, pp. 939–965, 2011.

[16] Y. Jiang, "High order finite difference multi-resolution weno method for nonlinear degenerate parabolic equations," *Journal of Scientific Computing*, vol. 86, pp. 1–20, 2021.

[17] M. Ahmat, S. Ni, M. Zhang, and Z. Zhao, "A sixth-order finite difference hweno scheme for nonlinear degenerate parabolic equation," *Computers & Mathematics with Applications*, vol. 150, pp. 196–210, 2023.

[18] P. Zhang and T. Xiong, "High order implicit finite difference schemes with a semi-implicit weno reconstruction for nonlinear degenerate parabolic equations," *Journal of Computational Physics*, vol. 467, p. 111442, 2022.

[19] C.-W. Shu and S. Osher, "Efficient implementation of essentially non-oscillatory shock-capturing schemes," *Journal of computational physics*, vol. 77, no. 2, pp. 439–471, 1988.